Original Article

Exosomal ITGB6 from dormant lung adenocarcinoma cells activates cancer-associated fibroblasts by KLF10 positive feedback loop and the TGF-β pathway

Xiang Feng[1], Xianling Liu[1], Juanjuan Xiang[2], Jiaqi Xu[2], Na Yin[2], Lujuan Wang[2], Chaoyuan Liu[1], Yuyao Liu[1], Tiantian Zhao[1], Zengyi Zhao[1], Yawen Gao[1]

[1]Department of Oncology, The Second Xiangya Hospital of Central South University, Changsha, China; [2]Cancer Research Institute, School of Basic Medical Science, Central South University, Changsha, China

Contributions: (I) Conception and design: Y Gao, X Feng, X Liu, J Xiang; (II) Administrative support: Y Gao, X Liu; (III) Provision of study materials or patients: C Liu, Y Liu, T Zhao, Z Zhao; (IV) Collection and assembly of data: J Xu, N Yin, L Wang; (V) Data analysis and interpretation: X Feng, J Xu, N Yin; (VI) Manuscript writing: All authors; (VII) Final approval of manuscript: All authors.

Correspondence to: Yawen Gao, MD. Department of Oncology, The Second Xiangya Hospital of Central South University, 139 Renmin Middle Road, Changsha 410000, China. Email: ygao6@csu.edu.cn.

Background: Dormant cancer cells are commonly known to play a pivotal role in cancer recurrence and metastasis. However, the mechanism of tumor dormancy and recurrence remains largely unknown. This study aimed to investigate the mechanism by which exosomes derived from dormant lung adenocarcinoma (LUAD) cells activate cancer-associated fibroblasts (CAFs) to reconstruct the extracellular matrix (ECM), providing a novel idea for decoding the mechanism of tumor dormancy.

Methods: In this study, high-dose cisplatin was used to induce the dormant LUAD cells. Exosomes were extracted from the culture supernatant of normal and dormant cancer cells. The effects of selected exosomal proteins on the fibroblasts were evaluated. RNA-seq for fibroblasts and exosomal proteomics for normal and dormant cancer cells were used to identify and verify the mechanism of activating fibroblasts.

Results: We demonstrated that exosomes derived from dormant A549 cells could be taken by fibroblasts. Exosomal ITGB6 transferred into fibroblasts induced the activation of CAFs by activating the KLF10 positive feedback loop and transforming growth factor β (TGF-β) pathway. High ITGB6 expression was associated with activation of the TGF-β pathway and ECM remodeling.

Conclusions: In all, we demonstrated that CAFs were activated by exosomes from dormant lung cancer cells and reconstruct ECM. ITGB6 may be a critical molecule for activating the TGF-β pathway and remodeling ECM.

Keywords: Lung cancer; dormancy; cancer-associated fibroblasts (CAFs); exosomes

Submitted Oct 31, 2023. Accepted for publication Dec 08, 2023. Published online Dec 14, 2023.
doi: 10.21037/tlcr-23-707
View this article at: https://dx.doi.org/10.21037/tlcr-23-707

Introduction

Platinum-based chemotherapy remains an integral treatment component of advanced non-small cell lung cancer (NSCLC) (1). Chemotherapy kills the vast majority of tumor cells; the residual cells enter into dormancy (2). Dormant tumor cells exhibit unique biological characteristics, including tumor microenvironment-dependence, cell cycle arrest, drug resistance after chemotherapy, immune escape, metastatic recurrence, and ability to resume proliferation (2,3). Dormant tumor cells are considered an important cause of cancer recurrence and metastasis (4,5). Nevertheless, the specific mechanism of tumor dormancy and recurrence is largely unknown (4,5).

Exosomes are lipid bilayer vesicles with a size of 30–150 nm in diameter. Exosomes are secreted from most cells,

containing, but not limited to, special proteins, nucleic acids, metabolites, and lipids (6,7). The structure of the lipid bilayer protects the bioactive substances from enzymatic degradation, maintaining the bioactive molecules carried (6,7). Thus, exosomes serve as 'transport carriers', which convey the contents of the exosomes into recipient cells as well as transmitting signals and substances over long distances (6-8). In the tumor microenvironment, exosomes serve as an important conduit for bidirectional communication between cells, transferring a variety of molecules from donor cells to recipient cells to modify the phenotype of microenvironments, such as immunosuppression, epithelial-mesenchymal transition, and extracellular matrix (ECM) remodeling (9,10).

The ECM is the non-cellular component of all tissues, consisting of over 300 unique matrix macromolecules, including collagens, proteoglycans, and glycoproteins (11). In the tumor microenvironment, ECM homeostasis is disrupted, resulting in a wide range of biochemical and physical changes, with significant effects on the transduction of cellular signals, matrix stiffness, tumor cell proliferation, and invasion (11-13). Cancer-associated fibroblasts (CAFs) are the main cell type in the tumor stroma which play pivotal roles in ECM remodeling (14-17). Various bioactive molecules derived from CAFs such as growth factors, cytokines, and ECM-modifying enzymes, remodel the ECM environment, which not only provides mechanical support for tumor cells but also promotes tumor cell proliferation, metastasis, and drug resistance (15,17-19). However, the molecular mechanisms by which cancer cells influence pro-metastatic matrix remodeling are still not fully understood.

A growing number of studies have demonstrated the correlation between CAFs and lung cancer (20-22). In the cohort of NSCLC patients who accepted tyrosine kinase inhibitors (TKIs) therapy, the function heterogeneity of CAFs depends on the activation of the intrinsic transforming growth factor β (TGF-β) pathway, which determined TKI treatment efficacy. The activation degree of TGF-β pathway had a positive correlation with the treatment efficacy (22). However, the other scRNA-seq study in NSCLC showed that two specific subtypes of CAFs were associated with T cell exclusion, by shaping dense and aligned fiber deposition to decreased T cell infiltration. T cell exclusion is the obstacle to improving T cell-based therapies and patient outcomes. One of the specific subtypes of CAFs shows the strong expression of TGFB1 (21). Besides, CAFs promote tumor progression by secreting growth factors, promoting EMT, remodeling ECM, and so on (20). However, the mechanism for the heterogeneity of CAFs and the role of different CAFs under different treatments may have remained largely unknown. In this study, we revealed a novel mechanism by which exosomes derived from dormant lung adenocarcinoma (LUAD) cells activate CAFs to reconstruct the ECM. We present this article in accordance with the MDAR reporting checklist (available at https://tlcr.amegroups.com/article/view/10.21037/tlcr-23-707/rc).

Highlight box

Key findings

- Exosomes derived from dormant lung adenocarcinoma (LUAD) cells promote the activation of cancer-associated fibroblasts (CAFs) and remodel the extracellular matrix. Exosomal ITGB6 from dormant LUAD cells activates transforming growth factor β (TGF-β) pathway and KLF10 positive feedback loop, which induces the activation of CAFs.

What is known and what is new?

- Dormant tumor cells are considered an important cause of cancer recurrence and metastasis. Nevertheless, the specific mechanism of tumor dormancy and recurrence is largely unknown.
- Exosomal ITGB6 derived from dormant LUAD cells was transferred into fibroblasts and induced the activation of a KLF10 positive feedback loop and the TGF-β pathway, which induced the activation of CAFs.

What is the implication, and what should change now?

- These findings have uncovered a novel perspective for the mechanisms underlying tumor relapse after chemotherapy.

Methods

Cell culture and tissue specimens

The human A549 cell line was obtained from the Cell Bank of Cancer Research Institute, Central South University (Changsha, China) and authenticated by short tandem repeat (STR) profiling (2022-08-03); the human MRC-5 cell line was purchased from the Cell Bank of Chinese Academy of Sciences (Shanghai, China; catalog number: GNHu4) and authenticated by STR profiling (2022-12-15). A549 was cultured in Roswell Park Memorial Institute (RPMI) 1640 medium (01-100-1A; Biological industries, Kibbutz Beit-Haemek, Israel) with 10% fetal bovine serum (FBS; 04-001-1A, Biological industries). MRC-5 was cultured in Minimal Essential Medium (MEM)-Eagle with 10% FBS (35-081-CV; Corning, NY, USA). Cells were sub-

cultured in 0.25% trypsin-EDTA (03-050-1A, Biological industries). All the cells were cultured at 37 ℃ in a 5% CO_2 atmosphere. Human tissue specimens were collected from The Second Xiangya Hospital, Central South University, China. Two patients had histologically confirmed LUAD, which received neoadjuvant chemotherapy but progressed. The first biopsy was performed before therapy to identify the tumor tissue type. After tumor progression, a second biopsy was performed for tumor gene sequencing to guide the next step of treatment. The study was conducted in accordance with the Declaration of Helsinki (as revised in 2013). The study was approved by the ethics review committee of The Second Xiangya Hospital (No. LYF20220103) and informed consent was taken from all the patients.

Dormant LUAD cells

The A549 cells were treated with cis-platinum to construct the model of dormant LUAD cells. Previous research has confirmed the reliability of the model for dormant cancer cells (23-25). Briefly, A549 cells were inoculated into a 10 cm dish for 24 hours before treatment. When the cell density reached 50–60%, cis-platinum was added into the medium at final concentration of 4.5 μg/mL. The medium was freshly replaced after 48 hours of incubation, and every 2 days thereon. After 16 days of incubation, the dormant LUAD cells were set up and collected for model validation or following experiments.

Exosome isolation

Before exosome isolation, FBS (04-001-1A, Biological industries) was centrifuged at 120,000 g for 16 hours to eliminate bovine exosomes (Avanti J-30I; Beckman Coulter, Brea, CA, USA). After high-speed centrifugation, the supernatant was collected and filtered through a 0.22 μm filtration membrane (Millipore, Burlington, MA, USA). A549 cells and dormant A549 cells were cultured in the medium with exosome-free FBS to eliminate external interference. After 48 hours, the culture medium was collected and cell debris removed by differential centrifugation of 300 g for 10 minutes, 2,000 g for 15 minutes, and 12,000 g for 30 minutes. The supernatant was filtered through a 0.22 μm filtration membrane (Millipore). Next, the ultimate supernatant was concentrated by centrifugal filtration at 5×10^3 g for 40 minutes at 4 ℃ with the ultrafiltration device (UFC900396, Millipore). Finally, exosome isolation reagent was mixed with the concentrated solution at a ratio of 1:5, and the follow-up steps of exosome isolation were performed according to the instructions (EXOTC50A-1, System Biosciences, Palo Alto, CA, USA). BCA™ Protein Assay Kit (CW0014S, CWBIO, Jiangsu, China) was used to measure exosomal protein. CD63 (EXOAB-CD63A-1, System Biosciences), TSG101 (EXOAB-TSG101-1, System Biosciences), and HSP 70 (EXOAB-Hsp70A-1, System Biosciences) were used as inner control for exosomes. The purified exosomes were either used immediately for subsequent experiments or stored at –80 ℃.

Transmission electron microscopy (TEM)

The purified exosomes were fixed with 1% glutaraldehyde for 10 minutes and washed with deionized water. Exosomes suspension (about 10 μL) was dripped on the formvar carbon coated 300-mesh copper electron microscopy grids (Agar Scientific Ltd., Stansted, UK), and incubated at room temperature for 5 minutes. Next, 2% uranyl oxalate was used to negatively stain the exosomes' sample for 1 minute at room temperature. The grids were rinsed thrice with phosphate-buffered saline (PBS) for 5 minutes each and air-dried for 5 minutes. The morphology of exosomes was observed by TEM (JEM-2100; JEOL, Tokyo, Japan). The experiment was independently repeated 3 times by biological replicates.

Nanoparticle tracking analysis (NTA)

The size distribution and concentration of exosomes were measured by NTA based on the instruction (Zetasizer Nano S/N 252 instrument; Particle Metrix, Maumelle, AR, USA). Exosomes were resuspended in 1 mL sterile 1× PBS. Diluted exosomes suspension was detected by Zetasizer Nano S/N 252 instrument based on Brownian motion and diffusion coefficients of particles. Sterile-filtered 1× PBS was used as a control. Samples were corrected with 1000-fold diluted CPC100 standard particles at the same setting. A total of five videos (60 seconds) of the moving particles were performed, and particle movement was analyzed by Software ZetaView 8.04.02 SP2 (Particle Metrix, Meerbusch, Germany). The experiment was independently repeated 3 times by biological replicates.

Cellular internalization of exosomes

To evaluate exosome internalization, exosomes were marked

with PKH67 following the instructions (MINI67-1KT; Sigma-Aldrich, St. Louis, MO, USA). Briefly, 1 mL Diluent C was mixed with 4 µL PKH67. Exosomes were incubated with the mixture for 5 minutes at room temperature. The reaction was terminated by added an equal volume of exosome-free FBS. Excess PKH67 was removed by washing twice with exosome-free FBS. Marked exosomes were incubated with MRC-5 when the cells density reached 80%. After incubation for 5 hours, the cells were washed twice with PBS, and fixed in 4% paraformaldehyde (PFA) for 30 minutes at room temperature. Next, the cells were incubated with 4',6-diamidino-2-phenylindole (DAPI; D9542; Sigma-Aldrich). After staining, MRC-5 cells which absorbed the marked exosomes were viewed by fluorescence microscope (BX53; Olympus, Tokyo, Japan). The experiment was independently repeated 3 times by biological replicates.

Exosome treatment

MRC-5 cells were inoculated into 6-well plates 24 hours before treatment. When the cell density reached 70–80%, exosomes (300 µg) were added into the culture medium per well. PBS was added to the control group. After 48 hours of incubation, cells were collected for the subsequent experiments.

Cell invasion assays

The invasive ability of the cells was assessed using the 24-well Transwell system (3422, Corning). Briefly, 60 µL of diluted Matrigel (about 1 mg/mL) was added to the upper chambers of transwells. The chambers were incubated at 37 ℃ for 30 minutes. The cell suspension was added into the upper chamber at a density of 5×10^4 cells per well. The complete medium was added to the bottom of 24-well plates. Next, the Transwell system was placed in the cell incubator for 48 hours. After incubation, the chambers were fixed in 4% PFA and 0.1% crystal violet ammonium oxalate solution (G1063; Solarbio, Beijing, China). A prewetted cotton swab was used to remove the cells coated on the inner side of the upper chambers. Cell invasion was viewed and photographed under microscope (CKX41, Olympus), and assessed by counting 6 random fields on the lower membrane surface. The experiment was independently repeated 3 times by biological replicates.

ECM-remodeling assay

To evaluate the matrix remodeling capability of fibroblasts, 1×10^6 MRC-5 cells incubated with exosomes were embedded in a 200 µL matrix mixture. The mixture was prepared as follows: Matrigel (354234, Corning), rat tail collagen type I (354236, Corning), and medium were mixed at a ratio of 1:2:2 by volume. Then, 1% 1M NaOH solution was added into the Matrigel mixture to adjust the pH. Next, mixtures with cells and Matrigel were seeded on a 24-well plate and incubated at 37 ℃ for 30 minutes. After the Matrigel mixture was set, 1 mL complete medium was added to each well. After 48 hours, gel contraction was accessed by taking pictures. ImageJ software (National Institutes of Health, Bethesda, MD, USA) was used to measure the gel contraction value, the formula was 100% × (1 – area of gel/bottom area). The practice was conducted with reference to previous studies (26-28). The experiment was independently repeated 3 times by biological replicates.

Cell transfection

si-KLF10, si-Smad2, and si-NC were synthesized by RiboBio (Guangzhou, China). MRC-5 cells were seeded in 6-well plates and cultured until they reached 60–70% confluence. Small interfering RNA (si-RNA; 100 nM) was mixed with Lipofectamine 3000 (L3000015; Thermo Fisher, Waltham, MA, USA) and used for transfection. The mixture was added to the cells and after 48 hours of incubation, transfected cells were collected and used for follow-up experiments.

KLF10 overexpression plasmid, Smad2 overexpression plasmid, ITGB6 overexpression plasmid, and empty vector plasmid were synthesized by GenScript (Nanjing, China). MRC-5 cells were cultured until they reached 90–100% confluence. After digestion, the cells were resuspended in opti-MEM medium. A mixture of plasmids and cells was prepared. Each electroporation cuvette was filled with 100 µL mixture containing 10 µg plasmid and 1×10^6 cells. A NEPA21 electrical transfection instrument was operated according to the manufacturer's instructions (NEPA GENE, Chiba, Japan). After transfection, the cells were transferred to 6-well plates and incubated with pre-warmed (37 ℃) complete medium. After 48–72 hours of incubation, transfected cells were collected and used for follow-up experiments. The experiment was independently repeated 3 times by biological replicates.

Western blotting

The radioimmunoprecipitation assay (RIPA) protein lysate (CW2333; CWBIO) containing protease inhibitors and phosphatase inhibitors was used to lyse the cells, and the total protein lysates were obtained. The protein quantification was performed using a bicinchoninic acid (BCA) Protein Quantitation Kit (CW0014S, CWBIO). Bio-Rad Bis-Tris Gel system (Bio-Rad, Hercules, CA, USA) was set up to perform the electrophoresis assay. Protein lysates were denatured and subjected to sodium dodecyl sulfate-polyacrylamide gel electrophoresis (SDS-PAGE). After that, gels were transferred to polyvinylidene fluoride (PVDF) membranes (Millipore). The membranes were blocked by 5% skimmed milk for 1.5 hours at room temperature. The primary antibody was diluted with Antibody Diluent Solution (P0023A; Beyotime, Haimen, China). The primary antibodies against α-SMA (alpha smooth muscle actin; 14395-1-AP; Proteintech, Rosemont, IL, USA), Vimentin [5741T; Cell Signaling Technology (CST), Danvers, MA, USA], KLF10 (ab184182; Abcam, Cambridge, UK), Smad2 (12570-1-AP, Proteintech), p-Smad2 (ab188334, Abcam), Smad3 (66516-1-Ig, Proteintech), and ITGB6 (28378-1-AP, Proteintech) were incubated overnight at 4 ℃. Anti-GAPDH antibody (10494-1-AP, Proteintech) was used as a loading control. Chemiluminescence signals were captured on Bio-Rad ChemiDoc XRS system (Bio-Rad). The experiment was independently repeated 3 times by biological replicates.

Quantitative real-time polymerase chain reaction (qRT-PCR)

Total RNA was extracted from cells by Trizol reagent (R401-01; Vazyme, Nanjing, China). RNA was reverse transcribed by HiScript II 1st Strand cDNA Synthesis Kit (R212-01, Vazyme). Glyceraldehyde-3-phosphate dehydrogenase (GAPDH) was used as the endogenous control to normalize expressions of the matrix-related molecules. The primers of the matrix related molecules were synthesized by Sangon Biotech (Shanghai, China). qRT-PCR was performed with the ChamQ Universal SYBR qRT-PCR Master Mix (Q711-02, Vazyme) using the Bio-Rad IQ^{TM}5 Multicolor Real-Time PCR Detection System (Bio-Rad). The experiment was independently repeated 3 times by biological replicates.

Immunohistochemistry

Tissue sections were routinely deparaffinized and hydrated, and antigens were repaired with sodium citrate solution. The sections were blocked with 3% H_2O_2 and 5% bovine serum albumin (BSA) solution, and the primary antibody was added and passed overnight at 4 ℃. The next day, sections were washed with PBS, dropped-added with secondary antibody and horseradish peroxidase (HRP), rested at 37 ℃ for 1 hour. The sections were washed with PBS, incubated with 3,3'-diaminobenzidine (DAB) solution for 10 minutes, washed with PBS, and counterstained with hematoxylin for 20 seconds. They were then dehydrated, sealed, and photographed. The experiment was independently repeated 3 times by biological replicates.

Statistical analysis

Data analysis was carried out using the software SPSS 20.0 (IBM Corp., Armonk, NY, USA. The graphs were made by GraphPad Prism 8.0 (GraphPad Software, San Diego, CA, USA). The comparisons between two group means were analyzed by *t*-test. The comparisons between multiple group means were analyzed by one-way analysis of variance (ANOVA), and any further significant difference between groups was determined using the Dunn multiple comparison test. A P value <0.05 was considered statistically significant.

Results

Exosomes derived from dormant LUAD cells reconstruct the ECM

To investigate the biological function of dormant tumor cells, we first constructed the model of dormant LUAD cells using human lung cancer line A549. Cell morphology was changed significantly after treatment, becoming spindle-shaped with loose intracellular connections (*Figure 1A*). Meanwhile, cells in the S phase population had been reduced and cells are arrested in the G0/G1 phase, suggesting that the cells had entered a dormant state (*Figure 1B,1C*). Compared to common cisplatin-resisted lung cancer cells, we used a short-term single dose of cisplatin instead of long-term repeated cisplatin treatment. Short-term treatment can induce temporary growth arrest and reenter the cell cycle after with drawl of chemotherapy. Previous study showed

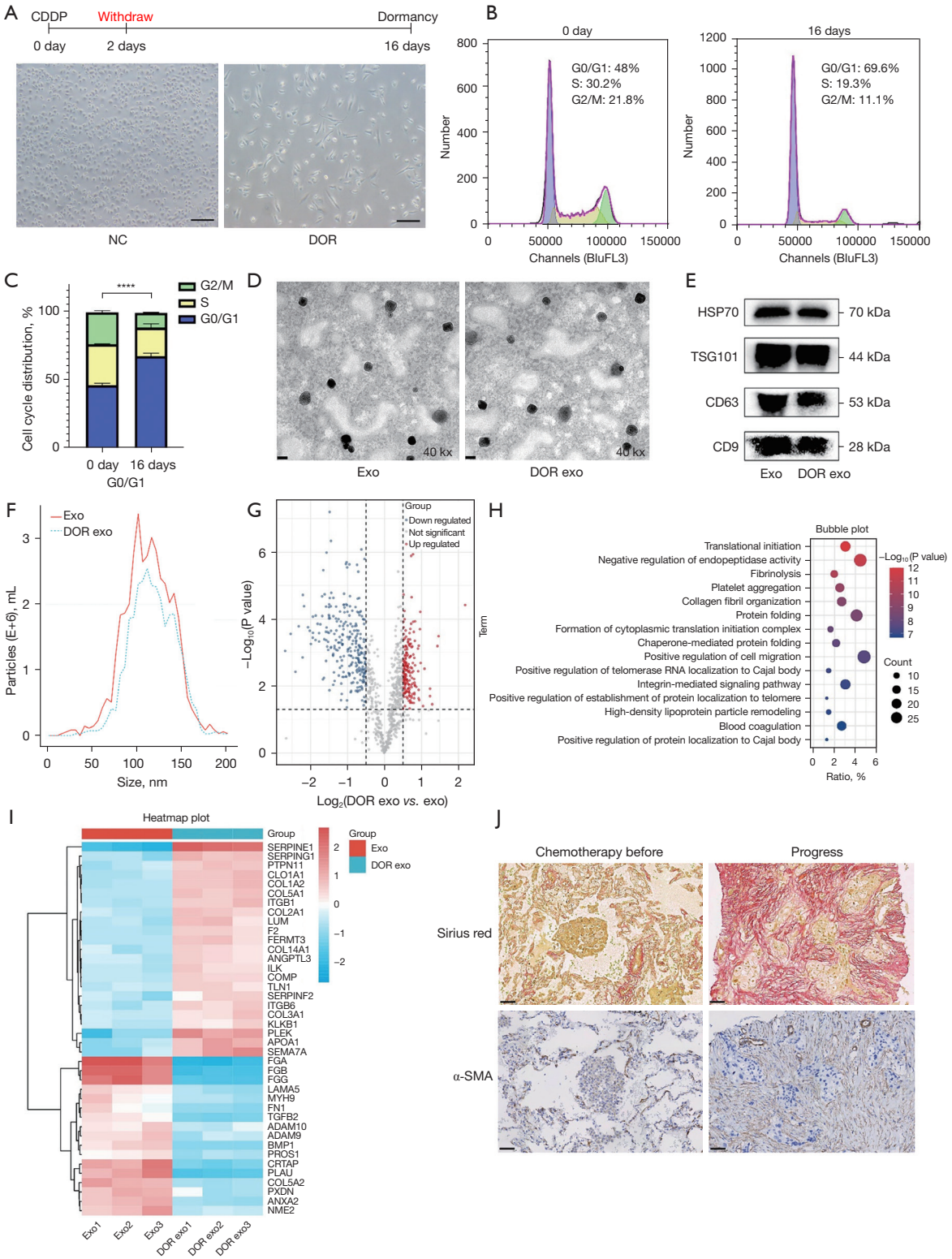

Figure 1 Exosomes derived from dormant LUAD cells reconstruct the ECM. A549 was treated with a high dose of cis-platinum for 2 days and cultured with fresh complete medium for 16 days. The treatment protocol is shown. (A) Cell morphology is shown in the pictures by inverted light microscope. Magnification: ×20; scale bar =400 μm. (B,C) Cell cycle assay suggested that the S phase population was reduced

and cells were arrested in the G0/G1 phase. (D) exo and DORexo were isolated and identified. The morphology of exosomes was observed by transmission electron microscopy. (E) Exosome-associated markers (HSP70, TSG101, CD63, and CD9) were detected by western blot. (F) Nanoparticle tracking analysis showed that the diameters of exosomes secreted from A549 cells and dormant A549 cells range from 50 to 170 nm. (G) The volcano plot shows differentially expressed proteins between exosomes derived from A549 cells and derived from dormant A549 cells (DORexo *vs*. exo). (H) GO functional enrichment analysis for differential expressed proteins from proteomics was performed and shown as a bubble map. (I) ECM-related proteins from GO enriched dataset were clustered and visualized as a heatmap. (J) Immunohistochemical analysis using the antibody against α-SMA evaluated the infiltration degree of α-SMA positive CAFs of one case of LUAD before treatment or with no chemotherapy response. Sirius red staining was performed to evaluate the degree of ECM remodeling. Magnification: ×100; scale bar =50 μm. ****, P<0.0001. CDDP, cisplatin; NC, A549 cells; DOR, dormant A549 cells; exo, A549-secreted exosomes; DORexo, dormant A549-secreted exosomes; α-SMA, alpha smooth muscle actin; LUAD, lung adenocarcinoma; ECM, extracellular matrix; GO, Gene Ontology; CAFs, cancer-associated fibroblasts.

that the surviving cells reinitiated to proliferate for an additional 16 days (24). A549-secreted exosomes (exo) and dormant A549-secreted exosomes (DORexo) were isolated respectively from the medium. Exosomes were observed by TEM (*Figure 1D*). Exosome-related biomarkers (HSP70, TSG101, CD63, and CD9) were detected by western blotting (*Figure 1E*). NTA showed that both diameters of exosomes derived from A549 and dormant A549 ranged from 50 to 170 nm (*Figure 1F*).

To explore the differences in protein components of the exosomes, we performed proteomics to screen for key molecules. After analysis, 578 proteins showed a difference in their expression levels (DORexo *vs.* exo), with 265 upregulated proteins and 313 downregulated proteins (*Figure 1G*). Besides, the expression of exosomal markers is different: exo (high expression of HSP90AA1, FN1 and LGALS3BP), DORexo (high expression of A2M, HBB, GSN, PRDX2 and RAP1B). Gene Ontology (GO) functional enrichment analysis for 578 proteins suggested that most of the enriched proteins mainly functioned in ECM remodeling (*Figure 1H*). Furthermore, 47 ECM-related proteins were clustered and visualized as a heatmap (*Figure 1I*). Taken together, these data indicated that exosomes derived from dormant A549 may regulate the process of reconstructing the ECM. Meanwhile, ECM remodeling was detected in LUAD after chemotherapy progress. Sirius red staining and immunohistochemical analysis showed that collagen deposition and the infiltration degree of α-SMA-positive CAFs were aggravated in progress state (*Figure 1J*).

Exosomes derived from dormant LUAD cells induce the activation of CAFs

To investigate whether DORexo are involved in ECM remodeling, we selected the human fibroblast MRC-5 for further investigation. MRC-5 cells were treated with PKH67-labeled exosomes. As shown in *Figure 2A*, the fluorescent exosomes entered the MRC-5 cells, suggesting that exosomes from cancer cells can translocate into recipient fibroblasts. The CAFs markers, such as α-SMA and Vimentin, were upregulated after treatment with DORexo compared to exo (*Figure 2B*). The expressions of CAFs-related molecules were verified by qRT-PCR, showing that *TGFB1*, *COL1A1*, and *COL3A1* were upregulated after treatment with DORexo compared to exo. Meanwhile, *COL4A1*, *IL-6*, and *IL-8* were downregulated (*Figure 2C*,*2D*). The cellular invasion was evaluated by transwell invasion assay. DORexo promoted the invasion of MRC-5 compared to exo (*Figure 2E*). The contractile ability of fibroblast was assessed by ECM-remodeling assay. DORexo improved the gel contraction capacity of fibroblast compared to exo (*Figure 2F*). In summary, these data indicated that DORexo induced the activation of CAFs with high expression of α-SMA, high invasive capability, and high contraction capacity, which was different from the observed effects of the exo group.

KLF10 is the key molecule for activating of CAFs

RNA sequencing was used to explore the molecular mechanism of activation of CAFs. The fibroblasts treated with exosomes were subjected to RNA sequencing. A heatmap analysis was conducted to evaluate the sequencing data. As shown in *Figure 3A*, 708 molecules showed a difference in their messenger RNA (mRNA) expression levels (DORexo *vs.* exo), with 457 upregulated molecules and 251 downregulated molecules (*Figure 3A*). We also included two independent datasets (GSE116679 and GSE61797) in the subsequent analysis. The Venn

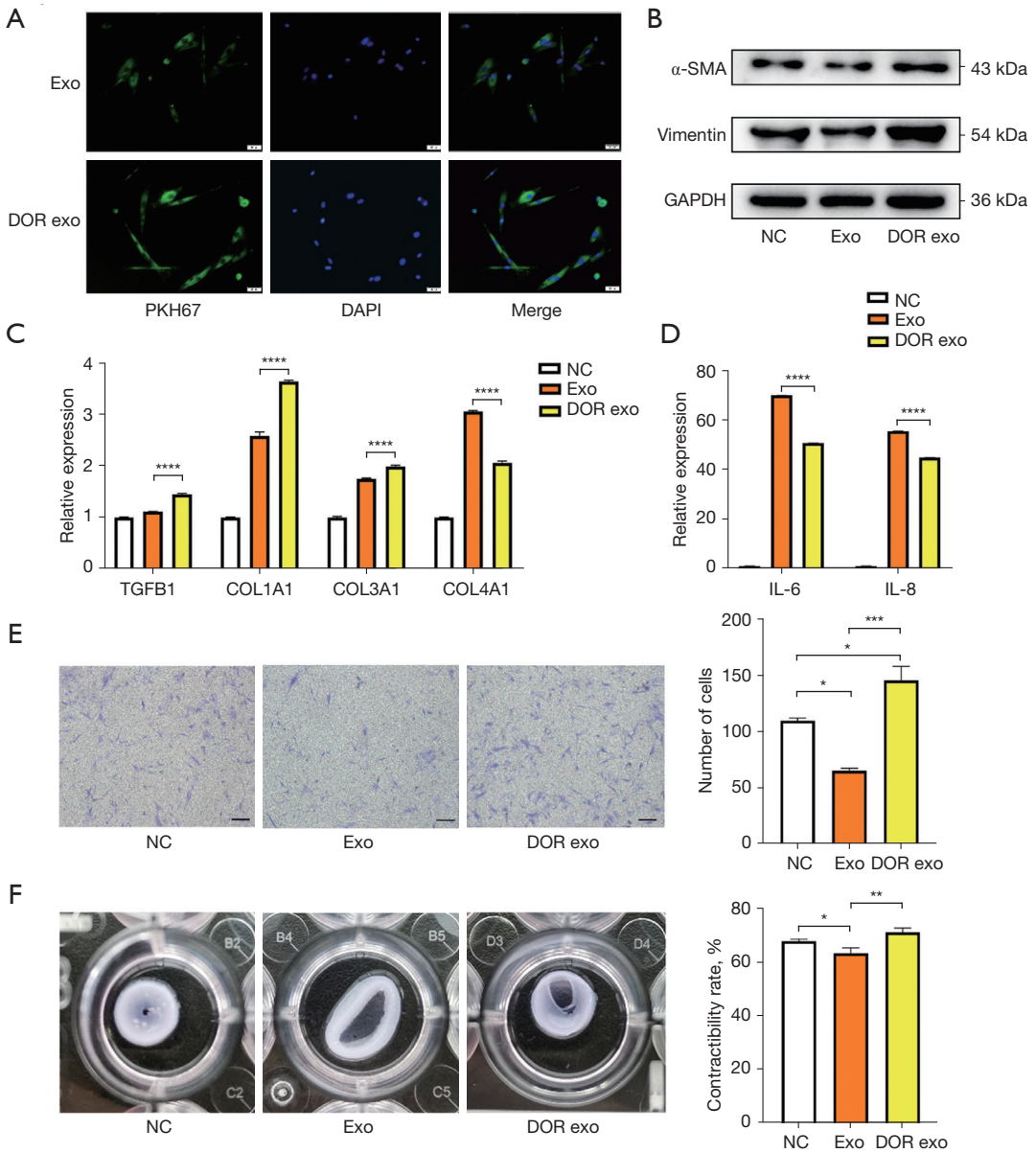

Figure 2 Exosomes derived from dormant LUAD cells induce the activation of CAFs. MRC-5 was selected as the research object and incubated with exosomes. (A) Immunofluorescence showed that exosomes marked with PKH67 were absorbed by MRC-5. Magnification: ×200; scale bar =50 μm. (B) MRC-5 was incubated with exosomes for 48 hours. Western blotting showed that the CAF markers (α-SMA and Vimentin) were upregulated after treatment with DORexo. (C) Matrix-related molecules in exosome-treated fibroblasts were measured by qRT-PCR. (D) Inflammation-related molecules in exosome-treated fibroblasts were measured by qRT-PCR. (E) The ability of invasion was evaluated by transwell assays. MRC-5 cells were treated with exosomes. Cells that invaded to the bottom surface were stained with crystal violet and observed by microscopy. Magnification: ×40; scale bar =200 μm. The numbers of invading cells were counted from 6 fields of view in each group. (F) The contractile ability of fibroblasts was assessed by ECM-remodeling assay. MRC-5 cells incubated with exosomes were embedded in a matrix mixture for 48 hours. Gel contraction was accessed by taking pictures. The formula for gel contraction value was 100 × (well diameter-gel diameter)/well diameter. Data were presented as the mean ± SD, and analyzed with one-way ANOVA. *, P<0.05; **, P<0.01; ***, P<0.001; ****, P<0.0001. exo, A549-secreted exosomes; DORexo, dormant A549-secreted exosomes; DAPI, 4',6-diamidino-2-phenylindole; NC, negative control; α-SMA, alpha smooth muscle actin; GAPDH, glyceraldehyde-3-phosphate dehydrogenase; LUAD, lung adenocarcinoma; CAFs, cancer-associated fibroblasts; qRT-PCR, quantitative real-time polymerase chain reaction; ECM, extracellular matrix; SD, standard deviation; ANOVA, analysis of variance; IL, interleukin.

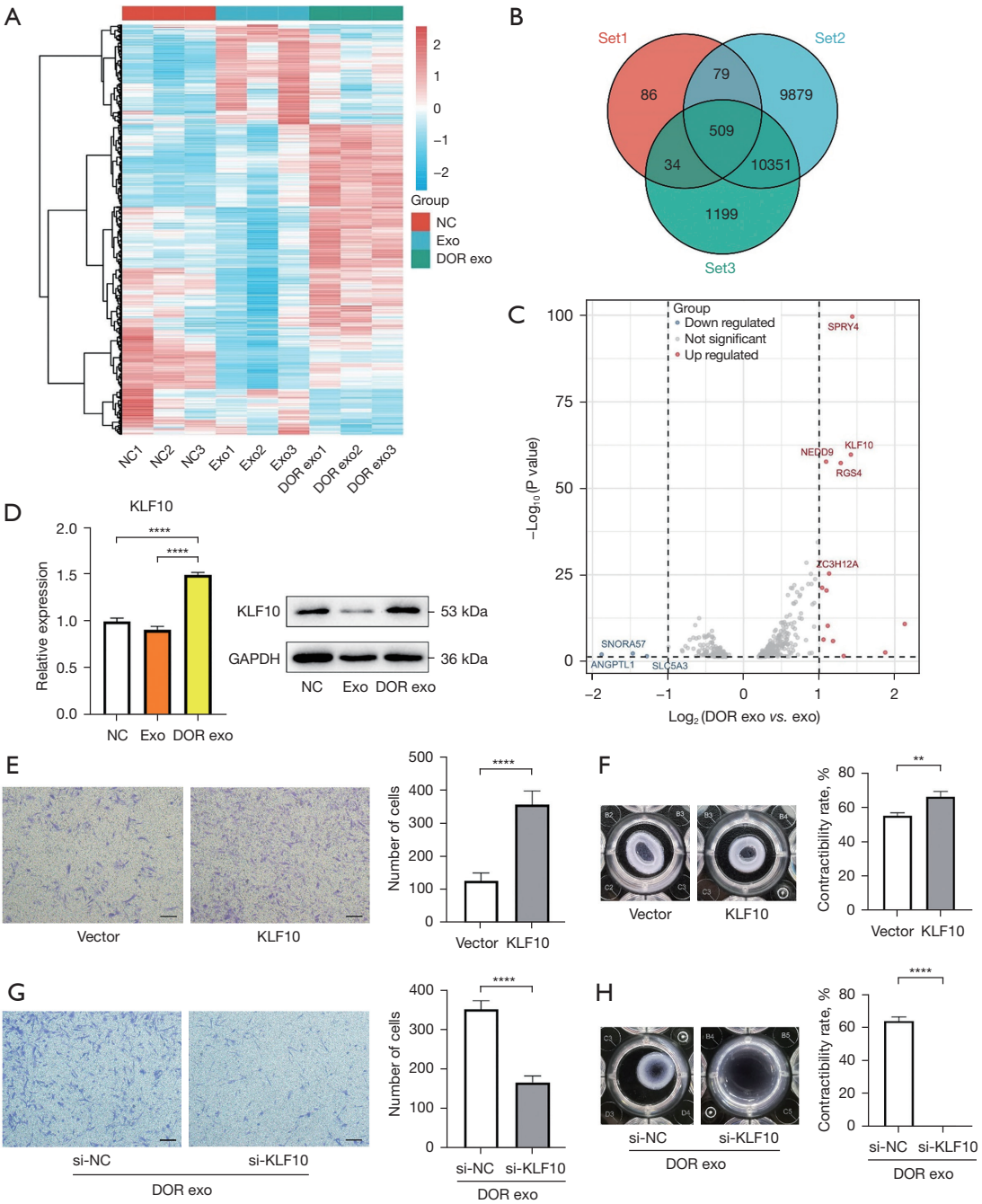

Figure 3 KLF10 is the key molecule for activation of CAFs. (A) The RNA expression profile of MRC-5 incubated with exosomes was examined. The heatmap of differentially expressed molecules was presented. (B) Venn diagram showing that the overlapping part between the 3 datasets contained 509 molecules, including our dataset and two independent datasets (GSE116679 and GSE61797). (C) The volcano plot for 509 molecules showed that KLF10 was one of the most representative differentially expressed RNA molecules. (D) The expression of KLF10 was measured by qRT-PCR and western blotting. (E,G) The invasion ability of fibroblast was accessed by transwell assays with crystal violet staining. Magnification: ×40; scale bar =200 μm. (F,H) The contractile ability of fibroblast was accessed by ECM-remodeling assay. Data are presented as the mean ± SD, and analyzed with Student's *t*-test. **, P<0.01; ****, P<0.0001. NC, negative control; exo, A549-secreted exosomes; DORexo, dormant A549-secreted exosomes; CAFs, cancer-associated fibroblasts; qRT-PCR, quantitative real-time polymerase chain reaction; ECM, extracellular matrix; SD, standard deviation.

diagram showed that the overlapping part between the three datasets included 509 molecules (*Figure 3B*). The volcano plot of 509 molecules displayed the representative differentially expressed RNA molecules. KLF10 was shown to be obviously upregulated in dormant exosome-treated fibroblasts (*Figure 3C*). The enhanced expression of KLF10 expression caused by DORexo in both mRNA and protein levels were confirmed by qRT-PCR and western blotting (*Figure 3D*). The KLF10 overexpression plasmid was transfected into MRC-5 using electrical transfection. An empty vector plasmid was transfected as the control. We found that the invasion and contractile ability of MRC-5 were increased by KLF10 overexpression (*Figure 3E,3F*). To assess the function of KLF10 in the process of activation of CAFs, we interfered expression of KLF10 using si-KLF10 (small interfering RNA targeting KLF10) in MRC-5 treated with DORexo. We used nonspecific siRNA as a control (si-NC). We found that KLF10 knock-down obviously inhibited the invasion and contractility caused by DORexo (*Figure 3G,3H*).

KLF10-Smad2 positive feedback loop induces the activation of CAFs by activating the TGF-β pathway

As we know, KLF10 can activate the TGF-β pathway via Smad2. We then examined if DORexo could activate the TGF-β pathway in MRC-5 cells through transferring KLF10. We observed that the TGF-β pathway was activated and accompanied by high expression levels of Smad2, Smad3, and p-Smad2 (*Figure 4A*). siRNA-mediated knockdown of KLF10 induced a significant decrease in expression levels of Smad2, Smad3, p-Smad2, and KLF10, whereas the expression levels of TGF-β pathway-associated proteins were rescued by KLF10 overexpression (*Figure 4B*). We also found that siRNA-mediated knockdown of Smad2 significantly suppressed the expression level of KLF10, whereas overexpression of Smad2 markedly increased the expression level of KLF10 (*Figure 4C*). This suggested that KLF10-mediated activation of CAFs is via activation of a KLF10-Smad2 positive feedback loop.

Exosomal ITGB6 from dormant LUAD cells induces the activation of CAFs by activating the TGF-β pathway

To uncover the mechanism of how the exosomes derived from dormant LUAD cells exert a pro-activation effect on CAFs, we analyzed the enriched proteins on exosomes which are related to the TGF-β pathway (GO:0007179) from the UniProt database. The Venn diagram showed that the overlapping part contained 12 molecules. ITGB6 was selected for further investigation (*Figure 5A*). ITGB6 was associated with the activation of TGF-β pathway which plays a pivotal role in matrix remodeling and fibrosis (29,30). ITGB6-mediated TGF-β activation is a major cause of fibrosis, including pulmonary fibrosis (31). Serum ITGB6 has been shown to be a marker for predicting the prognosis of cancer treatments, such as colorectal, gastric, and pancreatic cancers (32-34). Recently report showed that antibody-mediated inhibition of ITGB6 increased cytotoxic T cell infiltration by preventing tumor-promoting TGF-β activation to strengthen the efficacy of immune checkpoint inhibitors (35). Reviewing the proteomics, ITGB6 was highly expressed in DORexo compared with exo (*Figure 5B*). The western blot experiment validated the findings from the proteomics data (*Figure 5C*). After incubation with exosomes for 6 hours, MRC-5 was collected and used for subsequent western blotting. After a short processing time, we found that the DORexo increased the content of ITGB6 in MRC-5 compared to that of exo (*Figure 5D*). The findings revealed that exosomal ITGB6 was transported into MRC-5 by exosomes. To investigate the function of exosomal ITGB6 in MRC-5, we transfected an ITGB6 overexpression plasmid into MRC-5 using electrical transfection. After transfection, we found that overexpression of ITGB6 activated the TGF-β pathway and increased the expression levels of KLF10 (*Figure 5E*). Further, invasion and contractile ability were significantly increased in ITGB6 the overexpression group compared with the control group (*Figure 5F,5G*). To assess the correlation between the expression of ITGB6 and the progressive state of LUAD after chemotherapy, we found that the expression level of ITGB6 was increase in the progressive state (*Figure 5H*). Meanwhile, we evaluated the relationship between ITGB6 and the TGF-β pathway and ECM remodeling by searching the Tumor Immune Estimation Resource (TIMER2.0) database. We found that TGF-β associated receptors (*TGFBR1*, *TGFBR2*, and *TGFBR3*) and collagen (*COL1A1* and *COL4A4*) demonstrated a positive correlation with *ITGB6*. *COL2A1* showed a negative correlation with *ITGB6* (*Figure 6A,6B*). Taken together, ITGB6 may be a critical molecule for activating TGF-β pathway and remodeling ECM. In all, a proposed working model for this study was showed in *Figure 6C*.

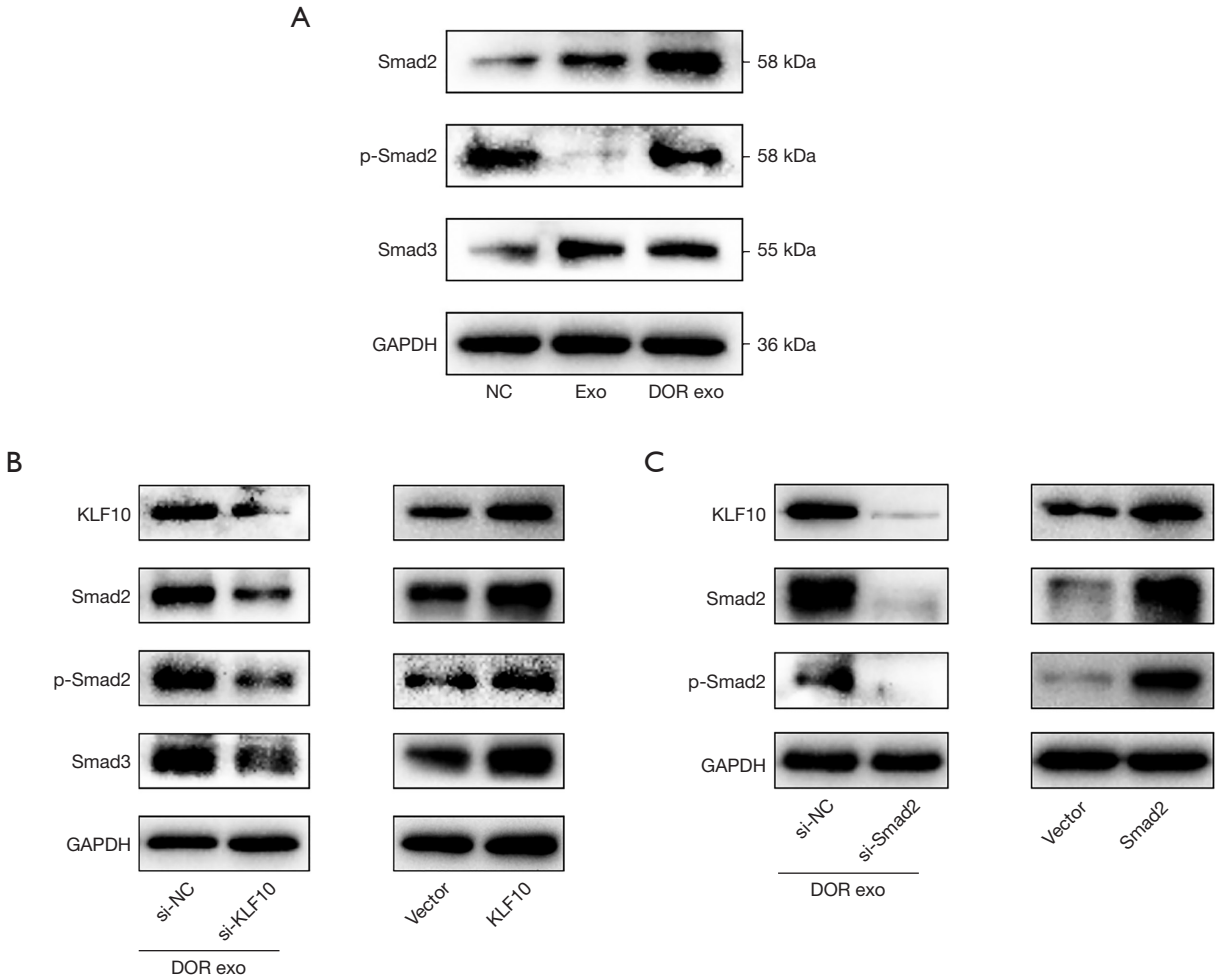

Figure 4 KLF10-Smad2 positive feedback loop induces the activation of CAFs by activating the TGF-β pathway. (A) Protein expression of the TGF-β pathway were measured by western blot analysis. MRC-5 cells were treated with DORexo compared to exo. GAPDH was used as the internal control. (B) Protein expression of KLF10 and TGF-β pathway were measured by western blot analysis. MRC-5 cells incubated with DORexo were transfected with si-KLF10. Further, MRC-5 cells were transfected with KLF10 overexpression plasmid. GAPDH was used as the internal control. (C) Protein expression of KLF10 and TGF-β pathway were measured by western blot analysis. MRC-5 cells incubated with DORexo were transfected with si-Smad2. Further, MRC-5 cells were transfected with Smad2 overexpression plasmid. GAPDH was used as the internal control. NC, negative control; exo, A549-secreted exosomes; DORexo, dormant A549-secreted exosomes; GAPDH, glyceraldehyde-3-phosphate dehydrogenase; CAFs, cancer-associated fibroblasts; TGF-β, transforming growth factor β.

Discussion

In this study, we show that exosomes derived from dormant LUAD cells promote the activation of CAFs and remodel the ECM. Exosomal ITGB6 from dormant LUAD cells activates TGF-β pathway and KLF10 positive feedback loop, which induces the activation of CAFs. We have uncovered a novel perspective for the mechanisms underlying tumor relapse after chemotherapy.

Exosomes, as an important pathway of bidirectional communication between cells, transport active molecules from the donor cell to the recipient cell, reprogram the tumor microenvironment, and participate in tumor progression (6,7). Exosomes derived from tumor cells contribute to reprogramming stromal cells to create a pro-tumor microenvironment, such as fibroblast (9,10). Exosomal miRNA-146a derived from breast cancer cells induces the activation of CAFs by downregulating TXNIP to active Wnt/β-catenin axis, which promotes breast

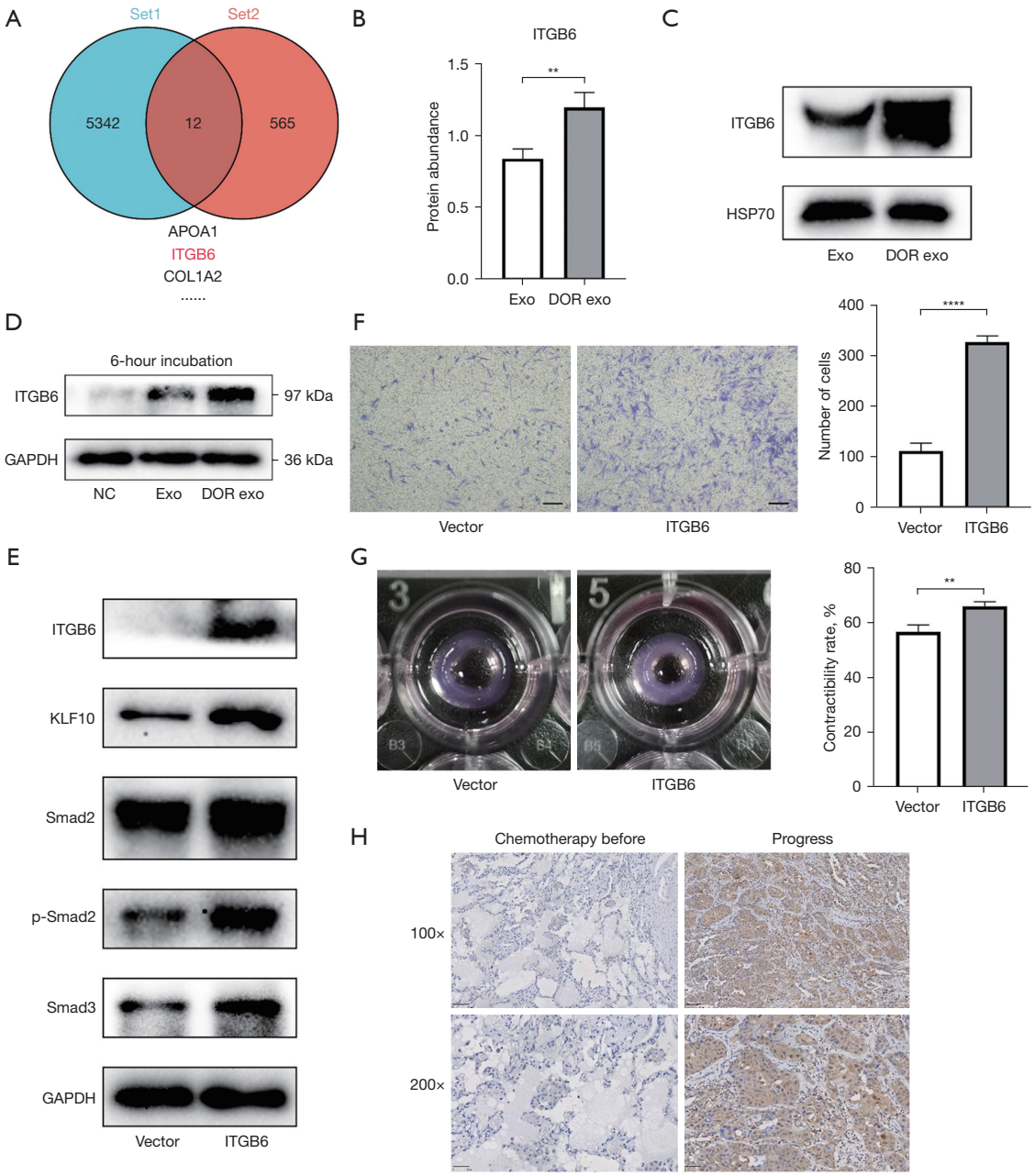

Figure 5 Exosomal ITGB6 from dormant LUAD cells induces the activation of CAFs by activating TGF-β pathway. (A) The Venn diagram showed that the overlapping part between the two datasets contained 12 molecules, including proteomics and TGF-β associated datasets (GO:0007179). ITGB6 was selected as the key molecule. (B) Proteomics showed that ITGB6 is up-regulation in DORexo. **, P<0.01. (C) ITGB6 was measured in DORexo by western blot analysis. (D) After brief processing (6 hours) with exosomes, the protein level of ITGB6 in MRC-5 cells was detected by western blot analysis. (E) Protein expression of ITGB6, KLF10, and the TGF-β pathway were measured by western blot analysis. MRC-5 cells were transfected with ITGB6 overexpression plasmid. (F,G) The invasion and contractile ability of fibroblast were accessed by transwell assays with crystal violet staining and ECM-remodeling assay. MRC-5 cells were transfected with ITGB6 overexpression plasmid. Magnification: ×40; scale bar =200 μm. **, P<0.01; ****, P<0.0001. (H) Immunohistochemical analysis evaluated the correlation between the expression of ITGB6 and progress state in one case of LUAD after chemotherapy. exo, A549-secreted exosomes; DORexo, dormant A549-secreted exosomes; NC, negative control; GAPDH, glyceraldehyde-3-phosphate dehydrogenase; LUAD, lung adenocarcinoma; CAFs, cancer-associated fibroblasts; TGF-β, transforming growth factor β; GO, Gene Ontology; ECM, extracellular matrix.

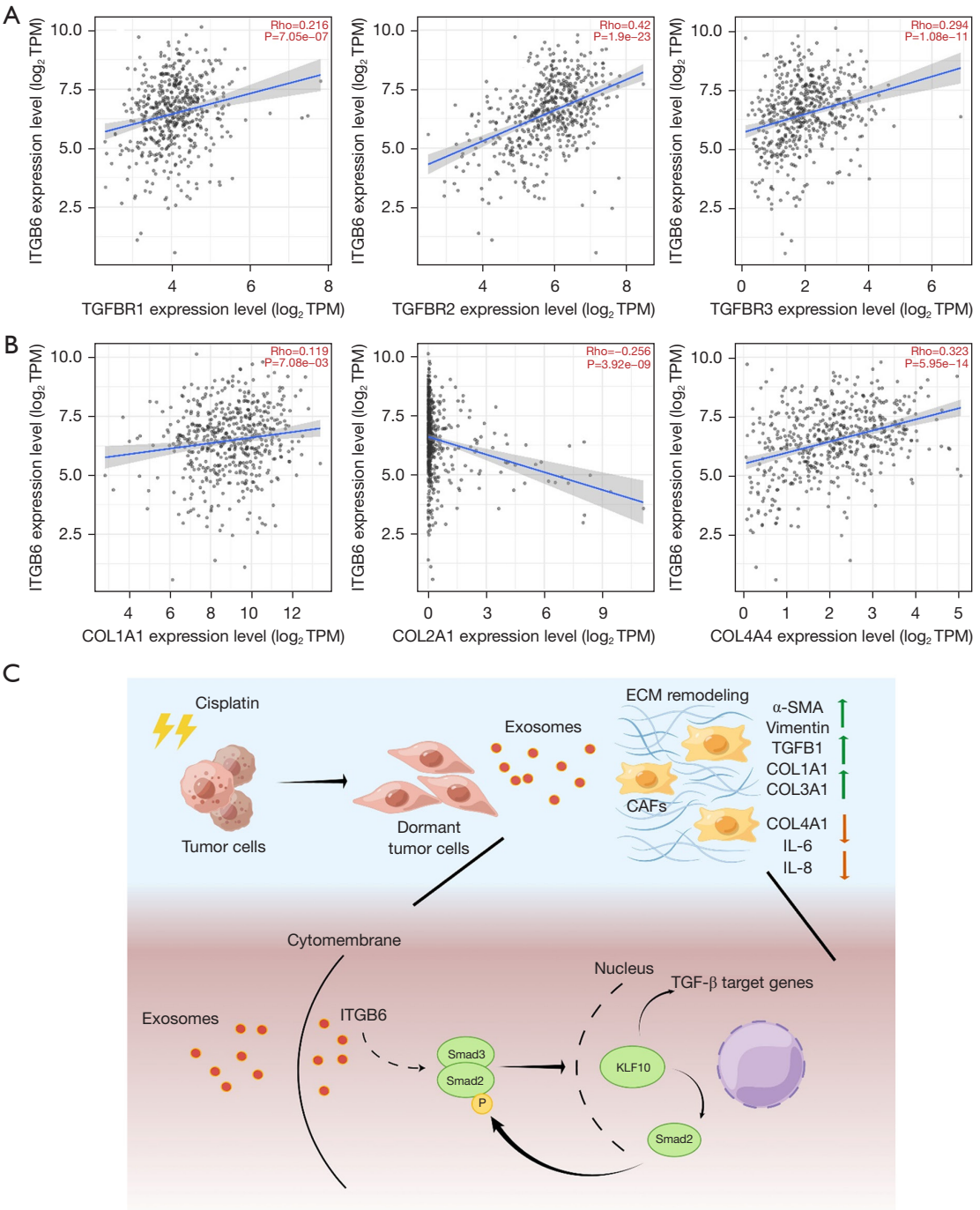

Figure 6 ITGB6 was associated with TGF-β pathway and ECM remodeling. (A) The correlation between ITGB6 and TGF-β pathway associated molecules was showed in LUAD patients by scatter diagram (TIMER2.0 database). (B) The correlation between ITGB6 and ECM-associated molecules in LUAD patients was shown by scatter diagram (TIMER2.0 database). (C) A proposed working model for exosomal ITGB6 derived from dormant LUAD cells was transferred into fibroblasts and induced the activation of a KLF10 positive feedback loop and the TGF-β pathway. The pattern diagram was drawn by Figdraw. TPM, transcripts per million; TGF-β, transforming growth factor β; ECM, extracellular matrix; CAFs, cancer-associated fibroblasts; α-SMA, alpha smooth muscle actin; IL, interleukin; LUAD, lung adenocarcinoma; TIMER2.0, Tumor Immune Estimation Resource.

cancer progression (36). In breast cancer, survivin derived from exosome actives fibroblasts by up-regulating SOD1 expression and transforms into myofibroblasts, which promotes the tumor progression (37). Exosomes derived from pancreatic cancer induce the infiltration of CAFs. Exosomal Lin28B was transferred to CAFs, which led to the upregulation of PDGFB (38). Similarly, exosomes derived from ovarian cancer cell-derived CAFs migration (39). In this study, we found that the markers of matrix remodeling were related to lung cancer progress after chemotherapy, and exosomes secreted by cisplatin-induces dormant LUAD cells transformed fibroblasts into CAFs.

CAFs mostly serve the pivotal pro-tumor role and promote the progression of tumors (40). The ECM characteristics of the metastatic microenvironment may determine the dormancy state of tumor cells (41,42). Integrin focal adhesion signaling is involved in the regulation of tumor cell dormancy-recovery (43). In breast cancer, cell adhesion molecule L1 (L1CAM) assist disseminated cancer cells to colonize the site of metastasis and translated from a dormant to a metastatic tumor by activating the integrin β1-ILK-YAP signaling in the perivascular mesenchymal cells (44). Integrin β1-FAK signaling axis activate the initial proliferation process of dormant tumor cells in lung (45). Discoidin domain receptors (DDRs) is one of the specialized transmembrane receptors which sense the changes in the biochemical and physical characteristics of ECM (46). The activation of non-canonical DDR1 signaling by TM4SF1 led to the activation of JAK2-STAT3 axis. SOX2 and NANOG were highly expressed on disseminated breast cancer cells, promoting their re-proliferation in the metastasis site of lung, bone, and brain tissue (47). Besides, tumor cell-derived ECM signaling is also involved in the process of tumor dormancy. A recent study showed that dormant cancer cells shape a type III collagen-rich ECM to maintain their dormancy. Mechanistically, the signaling of the type III collagen/DDR1/STAT1 pathway was identified, which keeps the dormancy state of cancer cells (42). However, relatively few studies have been reported associated with the role of tumor cell-derived ECM in tumor dormancy. In this study, we showed that exosomes derived from dormant LUAD cells induced the activation of CAFs, which may remodel the ECM and facilitate the process of dormancy-recovery.

CAFs are the main stromal cells around tumors which play an important role in reshaping the ECM environment (16,48). The remodeling of the ECM microenvironment by CAFs has been shown to induce interstitial sclerosis and fibrosis of interstitial cells, resulting in increased tissue tension (26,49). Increased tissue tension has been correlated to a poor prognosis for cancer (13,50). Studies have shown that several matrix molecules secreted from CAFs deposit in stroma, serving as a physical barrier to block tumor-infiltrating immune cells and participating in the process of immune escape (15,51). Matrix metalloproteinases for CAFs modify the ECM and assist tumor cell invasion (15). Notably, tumor cells migrate along the interspace shaped by contractile and proteolytic-mediated ECM remodeling forming migratory tracks for effective invasion; CAFs perform the role of guidance in this process (52). Further, the cellular population of CAFs is highly heterogeneous (53,54). A subset of α-SMA-positive CAFs shows the myofibroblastic phenotype which is known to enhance the abilities of constrict collagen fibers and increase the tissue tension (54,55). Inflammation associated CAFs—a poorly immunophenotypically characterized and IL-6-secreting CAFs subset—inhibit the activity of T cells and immune response (54,56). In this study, we found that CAFs treated with DORexo presented with a myofibroblastic phenotype accompanied by high expression of α-SMA, high gel contraction, and invasion capacity. The phenotype of the CAFs treated with DORexo seems to be more inclined to collagen deposition and ECM remodeling. In contrast, the subset of CAFs treated with exo seems to be more inclined to immunity regulation, with high expression of *IL-6* and *IL-8*. IL-6 and IL-8 were the signature inflammatory factors of the inflammatory CAFs (iCAFs), which might be involved in the process of tumor immunosuppression and progress by activating the STAT3 signaling pathway (56). Besides, the inflammatory factors secreted by CAFs participated in the regulation of the immune microenvironment. In pancreatic cancer, CAF-derived IL-6 played a key role in the recruitment of monocytes and facilitated the M2 polarization, IL-8 derived from CAFs performs a similar function (57,58). Moreover, CAF-derived IL-6 recruited and induced the dendritic cells in hepatocellular carcinoma to differentiate into regulatory dendritic cells that present little ability to express costimulatory molecules and present antigens (59). Other immune cells were influenced by iCAFs, such as T cells, mast cells, and NK cells (56). Furthermore, additional experiments are required to identify the characteristic of CAFs treated with exo.

Cancer-stromal interaction mediated by the TGF-β pathway has been recognized as an essential factor in tumor metastasis (60-62). High expression of TGF-β target genes in tumor stroma was associated with poor prognosis in

gastrointestinal cancer, such as gastric cancer and colorectal cancer (63). Further, CAFs are the primary influencing factor for the correlation between TGF-β signaling and poor prognosis (62,63). TGF-β derived from CAFs has been shown to reconstruct the ECM (62,64). The autocrine loop of TGF-β by CAFs induces a high expression of α-SMA, maintaining the progression of fibroblasts towards CAFs (60). Besides, the crosstalk between tumor cells and CAFs has been shown to maintaining the activation of CAFs by TGF-β pathway and corresponding target genes (65,66). A series of molecules including MMP1, FN1, and ITGB6 are involved in the activation of the TGF-β pathway, increasing the complexity further (67). In this study, DORexo transferred ITGB6 into MRC-5 and activated TGF-β pathway. We identified KLF10 as the key molecule of how dormant cancer cell exosomes induce the activation of CAFs. A KLF10 positive feedback loop plays a major role in activation of the TGF-β pathway and its downstream molecules (68). Overexpression of KLF10 in MRC-5 induces the transition from fibroblasts to CAFs, presenting an activated phenotype for ECM remodeling.

Targeting CAFs in cancer therapies showed promising therapeutic prospect benefits from a growing number of research findings. Scriptaid, a selective inhibitor of HDACs 1/3/8, was found to decrease the abundance of CAFs and inhibit the degree of ECM remodeling by the TGF-β pathway, which slows the growth of tumors (69). Pirfenidone is considered to be a potential treatment approach for targeting CAFs in breast cancer. Besides, pirfenidone decreased the expression of PD-L1 and reduced the release of CCL17 and TNF-β, which indicated that the immunosuppressive and invasiveness abilities of CAFs were weakened (70). A novel dendrimer conjugated with rapamycin was created to prevent fibroblast-mediated progression and metastasis in prostate cancer by inhibiting mTOR signaling and VEGF expression (71). CAF-targeted vaccines represent a viable option to fight against the cancer. The DNA vaccine targeting human FAPα induces FAPα-specific cytotoxic T lymphocyte responses, restraining the 4T1 tumor growth. Meanwhile, the expression of collagen I and various stromal factors that promote tumor progression was decreased due to the depletion of FAPα-positive CAFs (72). Furthermore, a dual-targeted DNA vaccine called OsFS was created which targets tumor cell antigen Survivin and CAFs marker FAPα simultaneously, improving the antitumor effect in a breast cancer model (73). Targeting CAF-derived ECM proteins could increase drug delivery to inhibit tumor growth by alleviating the ECM stiffness, such as fibronectin and hyaluronan (15,50,74). However, relevant clinical study results were not agreeable (15). The reason is that targeting the ECM component may be breaking the tissue homeostasis, which may aggravate the disease burden (15). The CAF-specific inhibitors have not been applied because of no markers specifically targeting fibroblasts are found. Further studies are required to reveal the specific pathway of fibroblast activation. In this study, we showed that exosomal ITGB6 is involved in the regulation of CAFs activation. Besides, ITGB6 was associated with TGF-β pathway and the expression of matrix components, indicating that ITGB6 may play a pivotal role in ECM remodeling. This finding may be a novel point for targeting CAFs and stroma in cancer therapies.

Conclusions

In this study, we found that exosomal ITGB6 derived from dormant LUAD cells was transferred into fibroblasts and induced the activation of a KLF10 positive feedback loop and the TGF-β pathway, which induced the activation of CAFs. The activated phenotype displayed the characteristics of myofibroblasts. Our study reveals a novel mechanism by which the exosomes derived from chemotherapy-induced dormant cancer cells activate CAFs and remodel the ECM.

Acknowledgments

Funding: This work was supported by National Natural Science Foundation, China (No. 82150006); Chinese Society of Clinical Oncology Research Foundation (Nos. Y-HR2017-117, Y-HH202102-0060); Beijing Medical and Health Foundation (No. YWJKJJHKYJJ-F3046D); Qujiang District Quzhou City Life Oasis Public Service Center (No. BJHA-CRP-040), Wu Jieping Medical Foundation (No. 320.6750.2023-05-10)

Footnote

Reporting Checklist: The authors have completed the MDAR reporting checklist. Available at https://tlcr.amegroups.com/article/view/10.21037/tlcr-23-707/rc

Data Sharing Statement: Available at https://tlcr.amegroups.com/article/view/10.21037/tlcr-23-707/dss

Peer Review File: Available at https://tlcr.amegroups.com/article/view/10.21037/tlcr-23-707/prf

Conflicts of Interest: All authors have completed the ICMJE uniform disclosure form (available at https://tlcr.amegroups.com/article/view/10.21037/tlcr-23-707/coif). The authors have no conflicts of interest to declare.

Ethical Statement: The authors are accountable for all aspects of the work in ensuring that questions related to the accuracy or integrity of any part of the work are appropriately investigated and resolved. The study was conducted in accordance with the Declaration of Helsinki (as revised in 2013). The study was approved by the ethics review committee of The Second Xiangya Hospital (No. LYF20220103) and informed consent was taken from all the patients.

References

1. Arbour KC, Riely GJ. Systemic Therapy for Locally Advanced and Metastatic Non-Small Cell Lung Cancer: A Review. JAMA 2019;322:764-74.
2. Maccalli C, Rasul KI, Elawad M, et al. The role of cancer stem cells in the modulation of anti-tumor immune responses. Semin Cancer Biol 2018;53:189-200.
3. Phan TG, Croucher PI. The dormant cancer cell life cycle. Nat Rev Cancer 2020;20:398-411.
4. Recasens A, Munoz L. Targeting Cancer Cell Dormancy. Trends Pharmacol Sci 2019;40:128-41.
5. Basu S, Dong Y, Kumar R, et al. Slow-cycling (dormant) cancer cells in therapy resistance, cancer relapse and metastasis. Semin Cancer Biol 2022;78:90-103.
6. Han QF, Li WJ, Hu KS, et al. Exosome biogenesis: machinery, regulation, and therapeutic implications in cancer. Mol Cancer 2022;21:207.
7. Lai JJ, Chau ZL, Chen SY, et al. Exosome Processing and Characterization Approaches for Research and Technology Development. Adv Sci (Weinh) 2022;9:e2103222.
8. Pegtel DM, Gould SJ. Exosomes. Annu Rev Biochem 2019;88:487-514.
9. Paskeh MDA, Entezari M, Mirzaei S, et al. Emerging role of exosomes in cancer progression and tumor microenvironment remodeling. J Hematol Oncol 2022;15:83.
10. Clancy JW, D'Souza-Schorey C. Tumor-Derived Extracellular Vesicles: Multifunctional Entities in the Tumor Microenvironment. Annu Rev Pathol 2023;18:205-29.
11. Popova NV, Jücker M. The Functional Role of Extracellular Matrix Proteins in Cancer. Cancers (Basel) 2022;14:238.
12. Werb Z, Lu P. The Role of Stroma in Tumor Development. Cancer J 2015;21:250-3.
13. Giussani M, Triulzi T, Sozzi G, et al. Tumor Extracellular Matrix Remodeling: New Perspectives as a Circulating Tool in the Diagnosis and Prognosis of Solid Tumors. Cells 2019;8:81.
14. Kalluri R. The biology and function of fibroblasts in cancer. Nat Rev Cancer 2016;16:582-98.
15. Chen X, Song E. Turning foes to friends: targeting cancer-associated fibroblasts. Nat Rev Drug Discov 2019;18:99-115.
16. Rimal R, Desai P, Daware R, et al. Cancer-associated fibroblasts: Origin, function, imaging, and therapeutic targeting. Adv Drug Deliv Rev 2022;189:114504.
17. Chhabra Y, Weeraratna AT. Fibroblasts in cancer: Unity in heterogeneity. Cell 2023;186:1580-609.
18. Jiang Y, Zhang H, Wang J, et al. Targeting extracellular matrix stiffness and mechanotransducers to improve cancer therapy. J Hematol Oncol 2022;15:34.
19. Guo Y, Li H, Sun C. Exosomal miR-125b-5p derived from cancer-associated fibroblasts promotes the growth, migration, and invasion of pancreatic cancer cells by decreasing adenomatous polyposis coli (APC) expression. J Gastrointest Oncol 2023;14:1064-76.
20. Shintani Y, Kimura T, Funaki S, et al. Therapeutic Targeting of Cancer-Associated Fibroblasts in the Non-Small Cell Lung Cancer Tumor Microenvironment. Cancers (Basel) 2023;15:335.
21. Grout JA, Sirven P, Leader AM, et al. Spatial Positioning and Matrix Programs of Cancer-Associated Fibroblasts Promote T-cell Exclusion in Human Lung Tumors. Cancer Discov 2022;12:2606-25.
22. Hu H, Piotrowska Z, Hare PJ, et al. Three subtypes of lung cancer fibroblasts define distinct therapeutic paradigms. Cancer Cell 2021;39:1531-1547.e10.
23. Li S, Kennedy M, Payne S, et al. Model of tumor dormancy/recurrence after short-term chemotherapy. PLoS One 2014;9:e98021.
24. Wang L, Peng Q, Yin N, et al. Chromatin accessibility

regulates chemotherapy-induced dormancy and reactivation. Mol Ther Nucleic Acids 2021;26:269-79.
25. Xu J, Feng X, Yin N, et al. Exosomes from cisplatin-induced dormant cancer cells facilitate the formation of premetastatic niche in bone marrow through activating glycolysis of BMSCs. Front Oncol 2022;12:922465.
26. Calvo F, Ege N, Grande-Garcia A, et al. Mechanotransduction and YAP-dependent matrix remodelling is required for the generation and maintenance of cancer-associated fibroblasts. Nat Cell Biol 2013;15:637-46.
27. Rath N, Morton JP, Julian L, et al. ROCK signaling promotes collagen remodeling to facilitate invasive pancreatic ductal adenocarcinoma tumor cell growth. EMBO Mol Med 2017;9:198-218.
28. Bertero T, Oldham WM, Grasset EM, et al. Tumor-Stroma Mechanics Coordinate Amino Acid Availability to Sustain Tumor Growth and Malignancy. Cell Metab 2019;29:124-140.e10.
29. Niu J, Li Z. The roles of integrin αvβ6 in cancer. Cancer Lett 2017;403:128-37.
30. Brown NF, Marshall JF. Integrin-Mediated TGFβ Activation Modulates the Tumour Microenvironment. Cancers (Basel) 2019;11:1221.
31. Puthawala K, Hadjiangelis N, Jacoby SC, et al. Inhibition of integrin alpha(v)beta6, an activator of latent transforming growth factor-beta, prevents radiation-induced lung fibrosis. Am J Respir Crit Care Med 2008;177:82-90.
32. Bengs S, Becker E, Busenhart P, et al. β6 -integrin serves as a novel serum tumor marker for colorectal carcinoma. Int J Cancer 2019;145:678-85.
33. Lenggenhager D, Bengs S, Fritsch R, et al. β6-Integrin Serves as a Potential Serum Marker for Diagnosis and Prognosis of Pancreatic Adenocarcinoma. Clin Transl Gastroenterol 2021;12:e00395.
34. Li Z, Sun Y, Xu J, et al. Integrin-β6 Serves as a Potential Prognostic Serum Biomarker for Gastric Cancer. Front Oncol 2021;11:770997.
35. Busenhart P, Montalban-Arques A, Katkeviciute E, et al. Inhibition of integrin αvβ6 sparks T-cell antitumor response and enhances immune checkpoint blockade therapy in colorectal cancer. J Immunother Cancer 2022;10:e003465.
36. Yang SS, Ma S, Dou H, et al. Breast cancer-derived exosomes regulate cell invasion and metastasis in breast cancer via miR-146a to activate cancer associated fibroblasts in tumor microenvironment. Exp Cell Res 2020;391:111983.
37. Li K, Liu T, Chen J, et al. Survivin in breast cancer-derived exosomes activates fibroblasts by up-regulating SOD1, whose feedback promotes cancer proliferation and metastasis. J Biol Chem 2020;295:13737-52.
38. Zhang YF, Zhou YZ, Zhang B, et al. Pancreatic cancer-derived exosomes promoted pancreatic stellate cells recruitment by pancreatic cancer. J Cancer 2019;10:4397-407.
39. Lee AH, Ghosh D, Quach N, et al. Ovarian Cancer Exosomes Trigger Differential Biophysical Response in Tumor-Derived Fibroblasts. Sci Rep 2020;10:8686.
40. Zhao Y, Shen M, Wu L, et al. Stromal cells in the tumor microenvironment: accomplices of tumor progression? Cell Death Dis 2023;14:587.
41. Kai F, Drain AP, Weaver VM. The Extracellular Matrix Modulates the Metastatic Journey. Dev Cell 2019;49:332-46.
42. Di Martino JS, Nobre AR, Mondal C, et al. A tumor-derived type III collagen-rich ECM niche regulates tumor cell dormancy. Nat Cancer 2022;3:90-107.
43. Balayan V, Guddati AK. Tumor Dormancy: Biologic and Therapeutic Implications. World J Oncol 2022;13:8-19.
44. Er EE, Valiente M, Ganesh K, et al. Pericyte-like spreading by disseminated cancer cells activates YAP and MRTF for metastatic colonization. Nat Cell Biol 2018;20:966-78.
45. Shibue T, Weinberg RA. Integrin beta1-focal adhesion kinase signaling directs the proliferation of metastatic cancer cells disseminated in the lungs. Proc Natl Acad Sci U S A 2009;106:10290-5.
46. Rammal H, Saby C, Magnien K, et al. Discoidin Domain Receptors: Potential Actors and Targets in Cancer. Front Pharmacol 2016;7:55.
47. Gao H, Chakraborty G, Zhang Z, et al. Multi-organ Site Metastatic Reactivation Mediated by Non-canonical Discoidin Domain Receptor 1 Signaling. Cell 2016;166:47-62.
48. Valkenburg KC, de Groot AE, Pienta KJ. Targeting the tumour stroma to improve cancer therapy. Nat Rev Clin Oncol 2018;15:366-81.
49. Caligiuri G, Tuveson DA. Activated fibroblasts in cancer: Perspectives and challenges. Cancer Cell 2023;41:434-49.
50. Laklai H, Miroshnikova YA, Pickup MW, et al. Genotype tunes pancreatic ductal adenocarcinoma tissue tension to induce matricellular fibrosis and tumor progression. Nat Med 2016;22:497-505.
51. Desbois M, Wang Y. Cancer-associated fibroblasts: Key

players in shaping the tumor immune microenvironment. Immunol Rev 2021;302:241-58.
52. Gaggioli C, Hooper S, Hidalgo-Carcedo C, et al. Fibroblast-led collective invasion of carcinoma cells with differing roles for RhoGTPases in leading and following cells. Nat Cell Biol 2007;9:1392-400.
53. Ishii G, Ochiai A, Neri S. Phenotypic and functional heterogeneity of cancer-associated fibroblast within the tumor microenvironment. Adv Drug Deliv Rev 2016;99:186-96.
54. Biffi G, Tuveson DA. Diversity and Biology of Cancer-Associated Fibroblasts. Physiol Rev 2021;101:147-76.
55. Tomasek JJ, Gabbiani G, Hinz B, et al. Myofibroblasts and mechano-regulation of connective tissue remodelling. Nat Rev Mol Cell Biol 2002;3:349-63.
56. Mao X, Xu J, Wang W, et al. Crosstalk between cancer-associated fibroblasts and immune cells in the tumor microenvironment: new findings and future perspectives. Mol Cancer 2021;20:131.
57. Nagarsheth N, Wicha MS, Zou W. Chemokines in the cancer microenvironment and their relevance in cancer immunotherapy. Nat Rev Immunol 2017;17:559-72.
58. Zhang R, Qi F, Zhao F, et al. Cancer-associated fibroblasts enhance tumor-associated macrophages enrichment and suppress NK cells function in colorectal cancer. Cell Death Dis 2019;10:273.
59. Cheng JT, Deng YN, Yi HM, et al. Hepatic carcinoma-associated fibroblasts induce IDO-producing regulatory dendritic cells through IL-6-mediated STAT3 activation. Oncogenesis 2016;5:e198.
60. Kojima Y, Acar A, Eaton EN, et al. Autocrine TGF-beta and stromal cell-derived factor-1 (SDF-1) signaling drives the evolution of tumor-promoting mammary stromal myofibroblasts. Proc Natl Acad Sci U S A 2010;107:20009-14.
61. Curran CS, Keely PJ. Breast tumor and stromal cell responses to TGF-β and hypoxia in matrix deposition. Matrix Biol 2013;32:95-105.
62. Fang Z, Meng Q, Xu J, et al. Signaling pathways in cancer-associated fibroblasts: recent advances and future perspectives. Cancer Commun (Lond) 2023;43:3-41.
63. Gough NR, Xiang X, Mishra L. TGF-β Signaling in Liver, Pancreas, and Gastrointestinal Diseases and Cancer. Gastroenterology 2021;161:434-452.e15.
64. Syed V. TGF-β Signaling in Cancer. J Cell Biochem 2016;117:1279-87.
65. Grubisha MJ, Cifuentes ME, Hammes SR, et al. A local paracrine and endocrine network involving TGFβ, Cox-2, ROS, and estrogen receptor β influences reactive stromal cell regulation of prostate cancer cell motility. Mol Endocrinol 2012;26:940-54. Erratum in: Mol Endocrinol 2014;28:275.
66. Calon A, Tauriello DV, Batlle E. TGF-beta in CAF-mediated tumor growth and metastasis. Semin Cancer Biol 2014;25:15-22.
67. Horiguchi M, Ota M, Rifkin DB. Matrix control of transforming growth factor-β function. J Biochem 2012;152:321-9.
68. Memon A, Lee WK. KLF10 as a Tumor Suppressor Gene and Its TGF-β Signaling. Cancers (Basel) 2018;10:161.
69. Kim DJ, Dunleavey JM, Xiao L, et al. Suppression of TGFβ-mediated conversion of endothelial cells and fibroblasts into cancer associated (myo)fibroblasts via HDAC inhibition. Br J Cancer 2018;118:1359-68.
70. Aboulkheyr Es H, Zhand S, Thiery JP, et al. Pirfenidone reduces immune-suppressive capacity of cancer-associated fibroblasts through targeting CCL17 and TNF-beta. Integr Biol (Camb) 2020;12:188-97.
71. Hill EE, Kim JK, Jung Y, et al. Integrin alpha V beta 3 targeted dendrimer-rapamycin conjugate reduces fibroblast-mediated prostate tumor progression and metastasis. J Cell Biochem 2018;119:8074-83.
72. Xia Q, Zhang FF, Geng F, et al. Anti-tumor effects of DNA vaccine targeting human fibroblast activation protein α by producing specific immune responses and altering tumor microenvironment in the 4T1 murine breast cancer model. Cancer Immunol Immunother 2016;65:613-24.
73. Geng F, Bao X, Dong L, et al. Doxorubicin pretreatment enhances FAPα/survivin co-targeting DNA vaccine anti-tumor activity primarily through decreasing peripheral MDSCs in the 4T1 murine breast cancer model. Oncoimmunology 2020;9:1747350.
74. Donelan W, Dominguez-Gutierrez PR, Kusmartsev S. Deregulated hyaluronan metabolism in the tumor microenvironment drives cancer inflammation and tumor-associated immune suppression. Front Immunol 2022;13:971278.

Cite this article as: Feng X, Liu X, Xiang J, Xu J, Yin N, Wang L, Liu C, Liu Y, Zhao T, Zhao Z, Gao Y. Exosomal ITGB6 from dormant lung adenocarcinoma cells activates cancer-associated fibroblasts by KLF10 positive feedback loop and the TGF-β pathway. Transl Lung Cancer Res 2023;12(12):2520-2537. doi: 10.21037/tlcr-23-707